Efficiency of osmotic pipe flows

Louise Sejling Haaning,[1,*] Kaare Hartvig Jensen,[1,2,*] Claus Hélix-Nielsen,[1] Kirstine Berg-Sørensen,[1] and Tomas Bohr[1,†]
[1]*Department of Physics, Technical University of Denmark, Kongens Lyngby, DK-2800, Denmark*
[2]*Department of Organismic and Evolutionary Biology, Harvard University, Cambridge, Massachusetts 02138, USA*
(Received 10 December 2012; published 28 May 2013)

We present experiments and theory for flows of sugar or salt solutions in cylindrical tubes with semipermeable walls (hollow fiber membranes) immersed in water, quantifying the strength of the osmotic driving force in relation to the dimensionless parameters that specify the system. The pumping efficiency of these flows is limited by the presence of "unstirred" concentration boundary layers near the tube walls, and our primary aim is to understand and quantify these layers and their effect on the flow. We measure the outlet flow rate Q_{out} while varying the inlet flow rate Q^*, concentration c^*, and tube length L, and map out the dependence of the flow rate gain $\gamma = Q_{\text{out}}/Q^* - 1$ on these parameters. A theoretical analysis based on (1) the known velocity field for slow flow in cylindrical porous tubes and (2) a parabolic concentration profile allows us to compute analytically how the flow gain depends on the relative magnitude of radial diffusion and advection as well as the ratio of the osmotic velocity to pumping velocity, in very good agreement with experiments and with no adjustable parameters. Our analysis provides criteria that are useful for optimizing osmotic flow processes in, e.g., water purification devices.

DOI: 10.1103/PhysRevE.87.053019 PACS number(s): 47.55.P−, 66.10.C−, 83.10.−y, 82.39.Wj

I. INTRODUCTION

Channel flows—liquid flows confined within a closed conduit with no free surfaces—are found in many natural and man-made systems. In animals [1] and plants [2] they serve as the building blocks of vascular systems, distributing energy to where it is needed and allowing distal parts of the organism to communicate. When constructed by humans, one of the major functions of channels is to transport liquids or gases, e.g., water (irrigation and urban water systems) and energy (oil or natural gas) from sites of production to the consumer or industry. In some cases, the channels have solid walls which are impermeable to the liquid flowing inside. In other cases, the channels have semipermeable membrane walls allowing solvent flux while rejecting solutes.

The effect of semipermeable porous walls is especially important in the study of biological flows due to the presence of semipermeable membranes and porous cell walls [2] and in industrial separation processes [3]. In these cases, the exchange of water across the membrane can be driven by either hydrostatic or osmotic pressure differences, thus modifying the bulk axial flow in the channel. A serious limitation to the performance of osmotic flows is that the entry of water into the tube lowers the solute concentration next to the membrane, as shown in Fig. 1. This negative feedback leads to a decrease in transmembrane flow that can affect the efficiency of both natural and engineered systems, such as sugar transport in the phloem vasculature of plants and water purification in filtration devices. Osmotic flows are exceptionally complicated to analyze due to the intrinsic nonlinear nature of the flow which arises due to the coupling between the velocity and concentration fields; see, e.g., [4–9]. Only in a few cases have experiments been compared directly to theory; see, e.g., [10–12].

In this article, we report experimental results for osmotic flows through a long, narrow cylindrical tube with porous walls. A simple continuum model predicts that the osmotic pumping efficiency is determined solely by two parameters: a Péclet number β (see Tables I and II for parameter definitions) and the maximal osmotic velocity scaled by the inlet velocity Γ. These parameters characterize the unstirred layer effects and the relative importance of feed and osmotic flows. Moreover, we observe that the pumping efficiency scales in an unexpected way with the parameters in the problem and show that our model correctly accounts for this scaling.

II. EXPERIMENTS

We flow aqueous solutions of sucrose ($C_{12}H_{22}O_{11}$) and sodium chloride (NaCl) through an experimental setup that consists of a long, narrow cylindrical hollow fiber membrane tube immersed in a reservoir containing pure water. It was fabricated by interfacial polymerization of a polyethersulfone substrate as described in [14,15], where the membrane used in this study is denoted the *B* type. A picture and a schematic sketch of the setup are shown in Fig. 2. We control the inlet flow rate by connecting the membrane tube to a syringe pump (Chemyx Inc., Fusion 400) and at the outlet, the solution flows into a reservoir at atmospheric pressure. The inlet flow rate and the solute concentration are varied over an order of magnitude: the flow rate from $Q^* = 0.2$ mm^3/s to $Q^* = 1.7$ mm^3/s and the concentration from $c^* = 0.05$ M to 1 M for NaCl and from $c^* = 0.05$ M to 0.5 M for sucrose. The radius of the tube is held constant at $a = 0.5$ mm, while the length of the tube is varied from $L = 6.2$ cm to $L = 13.6$ cm. This approach allows us to measure the flow rate gain due to osmotic influx, defined as the ratio of outlet to inlet volumetric flow rates,

$$\gamma = \frac{Q_{\text{out}}}{Q^*} - 1 = \frac{u_{\text{out}}}{u^*} - 1, \tag{1}$$

as a function of geometric and material properties of the problem. Here, Q_{out} and $u_{\text{out}} = Q_{\text{out}}/(\pi a^2)$ are the flow rate

*These authors contributed equally to this work.
†tbohr@fysik.dtu.dk

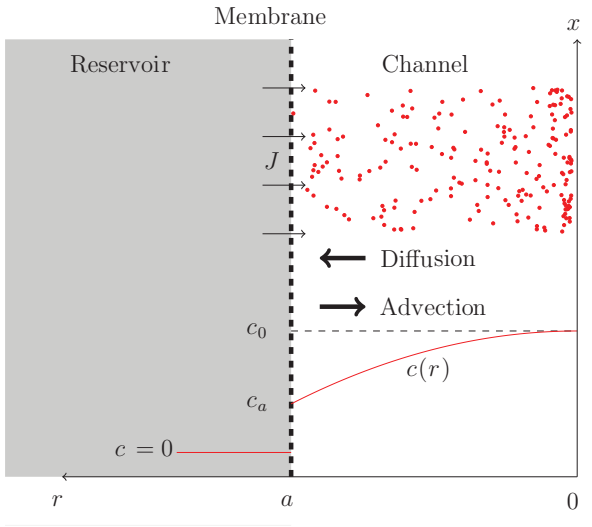

FIG. 1. (Color online) Sketch of the solute concentration $c(r)$ [solid red (gray) curve and density of dots] in a cylindrical tube of radius $r = a$ in contact with a reservoir containing pure solvent ($c = 0$). The semipermeable membrane separating the two solutions is indicated by the thick dashed line. The concentration difference between the reservoir and channel drives an osmotic flow of solvent $J \propto c_a$ [thin arrows; see Eq. (2)] across the membrane. This dilutes the solution next to the membrane, and the concentration of solute in contact with the membrane $c_a = c(a)$ is therefore lower than the value $c_0 = c(0)$ at the center of the tube. The concentration profile $c(r)$ is set by the relative magnitude of diffusive and advective fluxes (thick arrows). At the membrane interface ($r = a$), there can be no net flux of solute molecules $J_s = -D\partial_c + Jc_a = 0$, which determines the relative magnitude of c_0 and c_a; see Eq. (13).

and average axial velocity at the outlet, respectively, and $u^* = Q^*/(\pi a^2)$ is the average inlet velocity.

We use a balance (Sartorius CP 423S) to measure mass flow at the outlet. Typical flow rate gains vary over two orders of magnitude from $\gamma = 0.1$ to $\gamma = 10$. A representative experimental graph is shown in Fig. 3(a). Here, the effect of varying inlet flow rate at fixed solute concentration is illustrated. At large inlet flow rates, the solute is advected quickly through the tube and the osmotic flow has little effect. At low flow rates, however, we observe a strong gain. Similarly, Fig. 3(b) shows the effect of varying the solute concentration at fixed inlet flow rate. At low concentrations there is no net gain (i.e., $\gamma \ll 1$) since no osmotic flow occurs and we are simply observing the effect of the syringe pump. At $c^* = 1$ M,

TABLE I. Nondimensional parameters.

Aspect ratio	$\alpha = aL^{-1}$	0.004–0.008
Flow rate gain	$\gamma = Q_{\text{out}}(Q^*)^{-1} - 1$	0.1–10
Maximum flow rate gain	$\Gamma = 2L_pRTc^*L(u^*a)^{-1}$	0.08–20
Concentration variation	$\phi = (c_0 - c_a)/c_a$	0.04–1.1
Péclet number		
- axial	$\text{Pe}_x = u^*LD^{-1}$	10^3–10^5
- radial	$\text{Pe}_r = L_pRTc^*aD^{-1}$	0.3–3.9
- mixed	$\text{Pe} = u^*aD^{-1}$	68–2100
- boundary layer	$\beta = u^*a^2(6DL)^{-1}$	0.04–2.8
Reynolds number	$\text{Re} = \rho u^* a\eta^{-1}$	0.1–1

TABLE II. Material parameters at $T = 20\,^\circ$C. Values for D, R, and η were obtained from [13].

Tube radius	a	500 μm
Concentration at inlet	c^*	0.05 M – 1 M
Thickness of membrane tube wall	d	200 μm
Diffusion coefficient	D	5.2×10^{-10} m^2 s^{-1} (S)
		1.6×10^{-9} m^2 s^{-1} (NaCl)
Length of membrane tube	L	6.2 cm, 13.6 cm
Permeability of membrane	L_p	3.3×10^{-12} m s^{-1} Pa^{-1}
Flow rate at inlet	Q^*	0.2 – 2 mm^3 s^{-1}
Gas constant	R	8.314 J K^{-1} mol^{-1}
Absolute temperature	T	293 K
Velocity at inlet	u^*	60 – 600 μm s^{-1}
Viscosity	η	1 – 5 mPa s

however, the gain is significant ($\gamma \simeq 1$) and the axial flow in the membrane tube is strongly influenced by the osmotic pumping. To quantify the pumping process, we measure the gain as a function of inlet flow rate Q^*, and inlet solute concentration c^* for two different solutes, which yields a total of 216 data points, shown in Figs. 3(c) and 3(d).

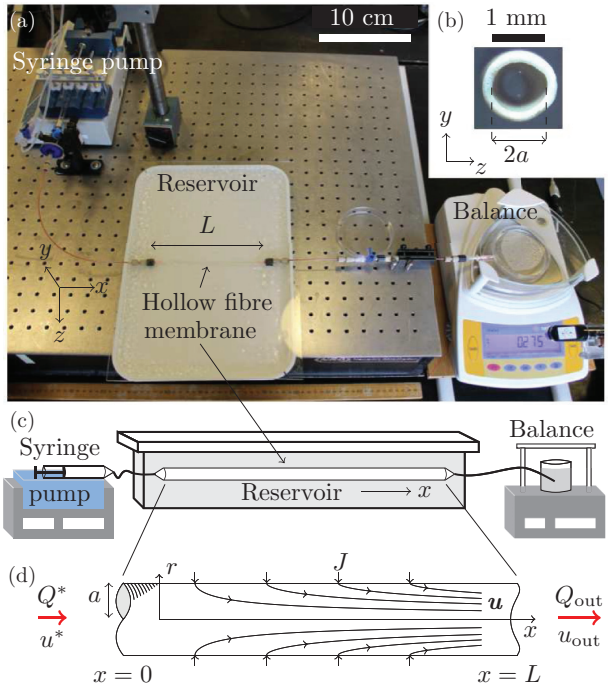

FIG. 2. (Color online) Experimental setup. (a) Picture of the experimental setup. The syringe pump injects an aqueous solution of NaCl or sucrose into the hollow fiber membrane tube which is immersed in a reservoir containing pure water. The flow along the x axis in the tube accelerates from the initial value Q^* due to osmotic exchange of water across the semipermeable wall. We measure the resulting outlet flow rate Q_{out} using a balance. (b) Cross sectional view of the hollow fiber membrane tube. The inner diameter of the tube is $2a = 1$ mm and the wall thickness is $d \simeq 200$ μm. (c) Schematic of the experimental setup. (d) Sketch of the cylindrical flow geometry. The velocity field $\boldsymbol{u}$ [streamline arrows; see Eqs. (5) and (6)] is determined by the average inlet flow velocity u^* and the transmembrane flux J.

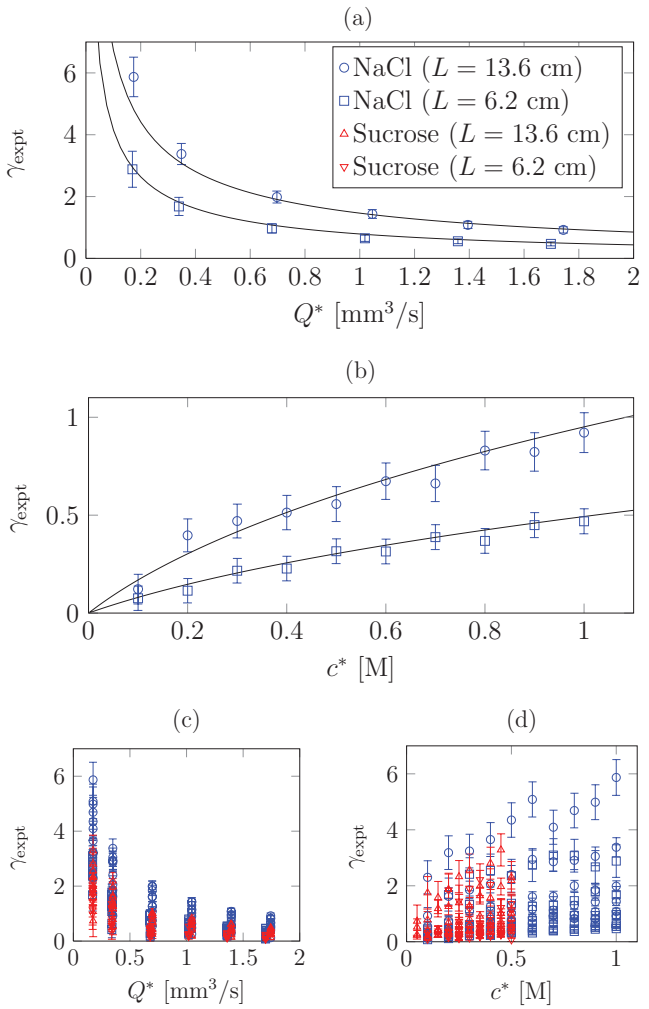

FIG. 3. (Color online) Experimental data, recorded with NaCl (a)–(d) and sucrose (c),(d) as the solute, as indicated in the legend of (a). (a) Flow rate gain $\gamma = Q_{\text{out}}/Q^* - 1$ plotted as a function of inlet flow rate Q^* for constant inlet NaCl concentration $c^* = 1.0$ M. (b) Flow rate gain γ plotted as a function of inlet NaCl concentration c^* for constant inlet flow rate $Q^* = 1.7$ mm^3/s. In (a) and (b), solid lines show theoretical predictions from Eq. (24) with no free parameters. In (c) and (d), experimental data from all 216 experiments using sucrose and NaCl are shown. Error bars in (a)–(d) indicate the errors obtained in the least squares fits to the slopes of the linear (time, mass) data curves measured using the balance shown in Fig. 2.

III. THEORY OF OSMOTIC PIPE FLOWS

As previously described, we propose that the flow of water across the membrane wall is driven by osmotic pressure differences with a modification due to the presence of concentration boundary layers. Aldis was the first to consider the effect of unstirred layers on osmotic flow in a cylindrical tube [11]. He found analytical solutions for the concentration and velocity fields in the limit of strong radial diffusion (boundary layer effects negligible) and for short distances using a series expansion. Our experiments, however, satisfy neither of these criteria and we proceed to analyze the problem in the general case.

We begin by writing the water flux J across the semipermeable tube wall as

$$J = L_p(RT\Delta c - \Delta p), \tag{2}$$

where L_p is the permeability of the membrane, R is the gas constant, T is the absolute temperature, Δc is the difference in solute concentration, and Δp is the difference in hydrostatic pressure between the inside and the outside of the tube. See the Appendix for details on how L_p was measured. For clarity we use the van't Hoff value $RT\Delta c$ for the osmotic pressure in Eq. (2), which is valid only for dilute (ideal) solutions. At the concentrations relevant to our experiments ($c < 1$ M for NaCl and $c < 0.5$ M for sucrose), the error in the osmotic pressure introduced by using the van't Hoff value is ~10% [16]. The liquid outside the tube is pure water ($c = 0$), so the concentration difference $\Delta c = c_a$, where c_a is the concentration at the inner surface of the tube ($r = a$; see Figs. 1 and 2). Viscous friction, which is responsible for the term Δp in Eq. (2), typically creates pressures of the order $\Delta p \simeq 8\eta u^* L/a^2 \simeq 1$ Pa where $\eta \simeq 1$–5 mPa s is the viscosity of the solution. These pressures are much smaller than the osmotic pressure differences $RT\Delta c \simeq 10^5$ Pa and it is therefore safe to disregard the Δp term in Eq. (2) and write instead $J = L_p RT c_a$.

The radial flux J of water in or out of the tube is naturally related to the mean axial flow velocity u along the x axis via volume conservation: $\partial_x u = 2J/a$. We therefore have the following equation for the average axial velocity

$$\partial_x u = 2\frac{L_p}{a} RT c_a. \tag{3}$$

The concentration c is governed by the advection-diffusion equation

$$\partial_t c + \mathbf{u}\cdot\nabla c = D\nabla^2 c, \tag{4}$$

where D is the diffusion coefficient of the solute in water (see Table II). The three-dimensional (3D) flow field $\mathbf{u} = (u_x, u_r, u_\theta)$ will generally be complicated, but since the channel Reynolds number $\text{Re} = \rho u^* a/\eta \simeq 0.1$ and aspect ratio $\alpha = a/L \simeq 0.005$ are both reasonably small we expect the flow to be rotationally symmetric and laminar and to have a Poiseuille axial flow profile. As shown by, e.g., Aldis [10], the velocity field $\boldsymbol{u} = (u_x, u_r)$ in cylindrical coordinates is then given by

$$u_x = 2\frac{(a^2 - r^2)}{a^2} u(x), \tag{5}$$

$$u_r = \frac{r(r^2 - 2a^2)}{a^3} J(x). \tag{6}$$

The hollow fiber membrane used in the experiments is able to retain ion-sized solutes. Moreover, axial diffusion plays very little role since the axial Péclet number $\text{Pe}_x = u^* L/D \simeq 10^4$ is large. Therefore, assuming steady state and taking the radial average of Eq. (4) implies that the axial solute flux is a conserved quantity, i.e.,

$$\langle cu \rangle = \text{const} = c^* u^*, \tag{7}$$

where $\langle cu \rangle = 2/a^2 \int_0^a u_x(r) c(r) r\, dr$. Of the concentration field $c(r,x)$ we know that the radial solute flux

$$J_c = -D\partial_r c + u_r c \tag{8}$$

must vanish at $r = 0$ and $r = a$ in order to satisfy the no-flux boundary condition at the channel center line and at the membrane wall. Equation (8) leads to

$$\partial_r c = 0 \quad \text{at} \quad r = 0, \tag{9}$$

$$-D\partial_r c - L_p RT c^2 = 0 \quad \text{at} \quad r = a. \tag{10}$$

When radial diffusion dominates, the difference in concentration across the tube will be small, specifically where the local Péclet number $J(x)a/D = L_p RT c_a(x)a/D$ is small. In this limit, it reasonable to assume that the concentration gradient at the membrane is of the order $(c_a - c_0)/a$, where $c_0(x)$ is the concentration at $r = 0$. To solve the averaged advection-diffusion equation (7), together with the boundary conditions in Eqs. (9) and (10), we approximate the concentration profile by a parabolic function

$$c(r) = c_0(x) + [c_a(x) - c_0(x)]\frac{r^2}{a^2}. \tag{11}$$

Since the advection-diffusion equation can be written entirely in terms of $\rho = r^2$,[1] we can safely neglect odd terms in r in the profile. The functional form of Eq. (11) is sketched in Fig. 1. In this approximation, the no-flux boundary condition at $r = a$ [Eq. (10)] is

$$-\frac{2D(c_a - c_0)}{a} - L_p RT c_a^2 = 0, \tag{12}$$

which sets a relation between the concentration at the channel center c_0 and wall c_a,

$$c_0 = c_a + \frac{L_p RT a}{2D}c_a^2 = c_a + \frac{\mathrm{Pe}_r}{2}\frac{c_a^2}{c^*}, \tag{13}$$

where $\mathrm{Pe}_r = L_p RT c^* a/D$ is the radial Péclet number.

From the conservation of solute flux [Eq. (7)], we now have from Eqs. (5) and (11)

$$\left(c_a + \frac{\mathrm{Pe}_r}{3}\frac{c_a^2}{c^*}\right)u = u^* c^*. \tag{14}$$

To eliminate c_a from Eq. (14) we use Eq. (3), which leads to

$$\left[\frac{a}{2L_p RT}\partial_x u + \frac{\mathrm{Pe}_r}{3c^*}\left(\frac{a}{2L_p RT}\partial_x u\right)^2\right]u = c^* u^*. \tag{15}$$

Introducing the variables $X = x/L$ and $U = u/u^*$, Eq. (15) can be written in nondimensional form

$$[\partial_X U + \beta\,(\partial_X U)^2]U = \Gamma, \tag{16}$$

where

$$\Gamma = 2\frac{L}{a}\frac{L_p RT c^*}{u^*} \tag{17}$$

is the ratio of the largest obtainable purely osmotic flow velocity $2\pi a L L_p RT c^*/(\pi a^2)$ and the inlet velocity u^*. The parameter

$$\beta = \frac{1}{6}\frac{a}{L}\frac{u^* a}{D} = \frac{1}{3}\frac{\mathrm{Pe}_r}{\Gamma} = \frac{1}{6}\alpha\mathrm{Pe} \tag{18}$$

is proportional to the ratio of the radial Péclet number Pe_r and the maximum flow gain Γ, or to the product of the aspect ratio α and the mixed Péclet number $\mathrm{Pe} = u^* a/D$.

In the nondimensional formulation, the flow rate gain is given by $\gamma = U(1) - 1$, and Γ thus provides an upper limit to the pumping efficiency, since we must have $\gamma \leqslant \Gamma$. An implicit solution of Eq. (16) can be obtained by the Legendre transformation $X = \partial_t y$, $U = t\partial_t y - y$, and $\partial_X U = t$. With this change of coordinates, Eq. (16) leads to a linear equation in $y(t)$,

$$(t^2 + \beta t^3)\partial_t y - (t + \beta t^2)y = \Gamma, \tag{19}$$

which has the solution

$$y(t) = \Gamma\left[-\frac{1}{2t} + \beta + t\beta^2 \ln\left(\frac{t}{1+\beta t}\right)\right] + tC \tag{20}$$

where the constant C allows us to fulfill the boundary condition $U(X(t) = 0) = 1$ [in dimensional coordinates $u(0) = u^*$]. The nondimensional velocity $U(X(t))$ and axial coordinate $X(t)$ can be written in terms of t as

$$X = \Gamma\left[\frac{1}{2t^2} + \frac{\beta^2}{1+\beta t} + \beta^2 \ln\left(\frac{t}{1+\beta t}\right)\right] + C, \tag{21}$$

$$U = \frac{\Gamma}{t + \beta t^2}. \tag{22}$$

To determine C, we note that $U = 1$ when $t = t_0 = (-1 + \sqrt{1 + 4\Gamma\beta})/(2\beta)$. By inserting t_0 in Eq. (21) with $X = 0$, we find that

$$C = -\Gamma\left[\frac{1}{2t_0^2} + \frac{\beta^2}{1+\beta t_0} + \beta^2 \ln\left(\frac{t_0}{1+\beta t_0}\right)\right]. \tag{23}$$

The flow rate gain γ can finally be determined from

$$\gamma(\beta,\Gamma) = U(1) - 1 = \frac{\Gamma}{t_1 + \beta t_1^2} - 1, \tag{24}$$

where t_1 is found from Eq. (21) by solving $X(t_1) = 1$.

The flow rate gain γ predicted by Eq. (24) is plotted as a function of β and Γ in Fig. 4(a). In Fig. 4(b), it is compared to measured values of γ from 216 experiments. Over two orders of magnitude of variation in γ, we find excellent agreement between the experimental data and the prediction of Eq. (24) with no free parameters.

When deriving Eq. (24), we approximated the concentration by the parabolic profile given in Eq. (11) under the assumption that the radial concentration distribution was close to uniform. To check this condition we consider the magnitude of $\phi = (c_0 - c_a)/c_a$. If $\phi = 0$, the concentration profile is completely flat while if $\phi = 1$ the concentration varies by a factor of 2 across the tube. Using Eqs. (13), (3), and (16), ϕ can be written as

$$\phi = \frac{c_0 - c_a}{c_a} = \frac{3}{4}\left(\sqrt{1 + \frac{4}{3}\frac{\mathrm{Pe}_r}{U}} - 1\right). \tag{25}$$

[1]It can be shown that the advection-diffusion equation $\boldsymbol{u}\cdot\nabla c = D\nabla^2 c$ can be written in terms of $\rho = r^2$ and that one can write a power series expansion of $c(r,x)$ containing only even powers of ρ.

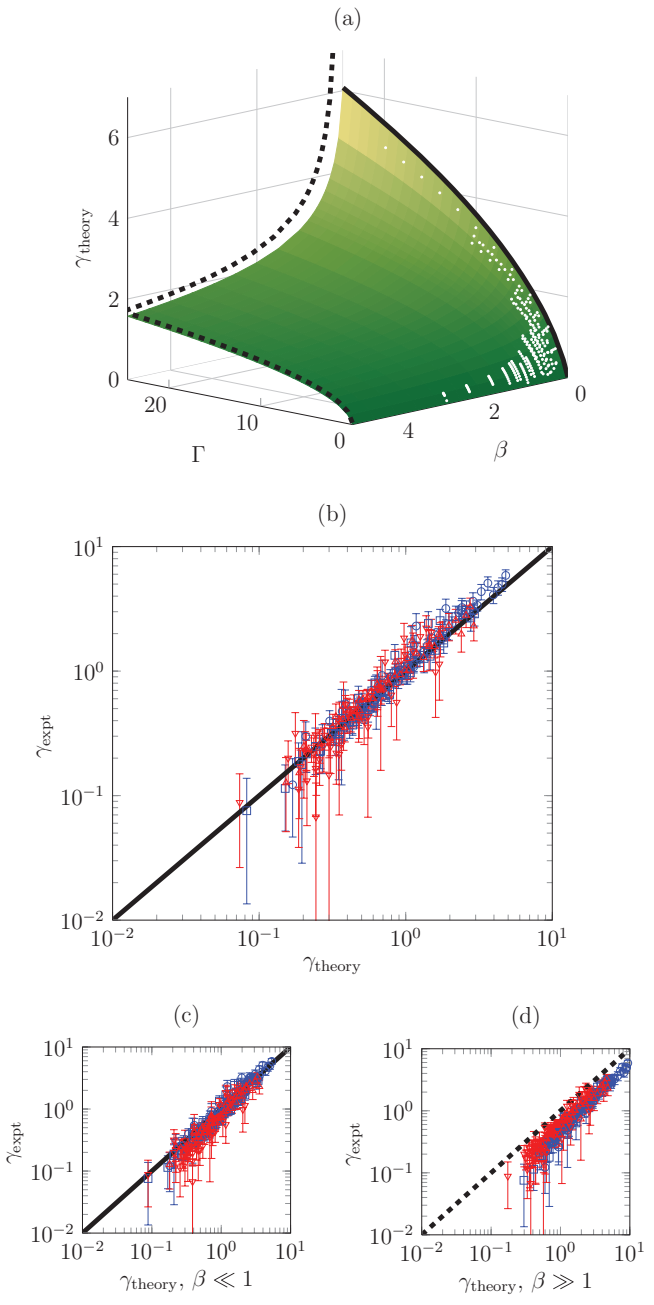

FIG. 4. (Color online) Comparison between experimental and theoretical values of the flow rate gain γ. (a) Green (gray) surface shows theoretical predicted values of γ [Eq. (24)] plotted as a function of β and Γ. The solid black line indicates the approximate analytical solutions for $\beta \ll 1$ [Eq. (28)]. The black dashed lines indicate the approximate analytical solutions for $\beta \gg 1$ [Eq. (30)]. White dots indicate the location in the (β,Γ) plane of experimental data points. (b) Measured values of γ plotted as a function of the predicted values using Eq. (24). (c) Measured values of γ plotted as a function of the predicted values using Eq. (28). (d) Measured values of γ plotted as a function of the predicted values using Eq. (30). (b)–(d) use the same legend as Fig. 3(a).

In a given experiment, the nondimensional velocity $U = u/u^*$ varies between 1 and $\gamma + 1$ along the tube [see Eq. (1)]. This observation leads to the following inequality for ϕ:

$$\frac{3}{4}\left(\sqrt{1+\frac{4}{3}\frac{\mathrm{Pe}_r}{1+\gamma}}-1\right) < \phi < \frac{3}{4}\left(\sqrt{1+\frac{4}{3}\mathrm{Pe}_r}-1\right). \tag{26}$$

Using measured values of γ and calculated values of Pe_r, we find that ϕ varies between 0.04 and 1.1, indicating that there is at most a 50% variation in concentration across the tube, in rough accord with the slowly varying concentration approximation.

A. Limiting cases

In the majority of our experiments, both β and Γ are of moderate magnitude [see Fig. 4(a) and Table II]. It is therefore likely that the boundary layer contributes significantly to the flow and that the full solution of Eq. (16) is needed to rationalize the experimental data. It is, however, of general interest to consider limiting cases of Eq. (16) and we therefore consider below solutions for $\beta \ll 1$ and $\beta \gg 1$ for arbitrary values of Γ. Taking $\Gamma \ll 1$ leads to $u(x) = u^*$ (i.e., $\gamma = 0$), and is therefore of limited interest since we generally look for conditions that optimize the osmotic flow and thus maximize γ.

1. *Weak unstirred concentration boundary layer effects*

Consider the situation where radial diffusion is strong compared to both radial and axial advection. In this case the radial and mixed Péclet numbers $\mathrm{Pe}_r = L_p RTc^* a/D$ and $\mathrm{Pe} = u^* a/D$ are small. This implies (i) that the concentration is nearly uniform [$\phi \sim \mathrm{Pe}_r \ll 1$; see Eq. (25)], and (ii) that the parameter $\beta \sim \alpha\mathrm{Pe} \ll 1$ [see Eq. (18)] when the aspect ratio $\alpha = a/L$ is small, as is generally the case in our experiments. In this limit, the solution of Eq. (16) is

$$U(X) = (1 + 2\Gamma X)^{1/2}, \tag{27}$$

which has previously been found by, e.g., Aldis [11] and Thompson and Holbrook [17]. In this limit, the flow rate gain γ can be expressed as

$$\gamma + 1 = (1 + 2\Gamma)^{1/2} = \left(1 + \frac{4L_p RTc^*}{u^*}\frac{L}{a}\right)^{1/2}, \tag{28}$$

shown in Fig. 4(a) as a solid line. Equation (28) provides a useful approximation to γ for small values of β.

2. *Strong unstirred concentration boundary layer effects*

When radial diffusion becomes comparable to or weaker than radial and axial advection, both the radial and the mixed Péclet numbers $\mathrm{Pe}_r = L_p RTc^* a/D$ and $\mathrm{Pe} = u^* a/D$ can become greater than 1. In this limit the concentration profile in the tube is no longer uniform [$\phi \geqslant 1$; see Eq. (25)] and the magnitude of the parameter β can exceed unity. Keeping in mind that that our experiments have confirmed the validity of Eq. (16) only for $\beta \leqslant 2.8$, we proceed to consider the case $\beta \gg 1$. In this limit, the solution of Eq. (16) is

$$U(X) = \left[\frac{3}{2}\left(\frac{\Gamma}{\beta}\right)^{1/2} X + 1\right]^{2/3}. \tag{29}$$

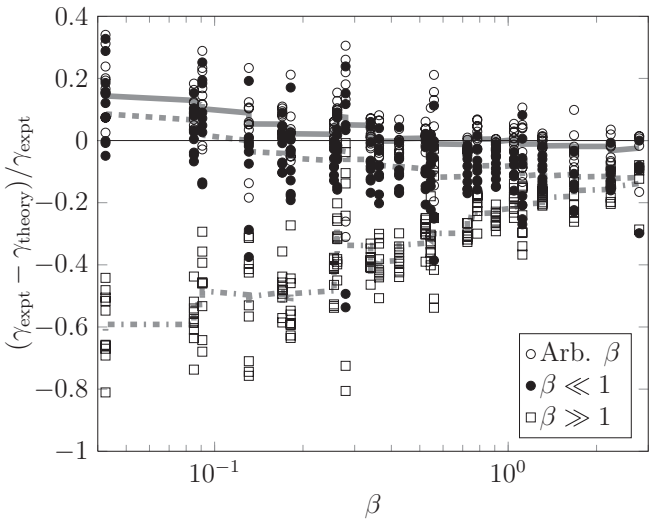

FIG. 5. Comparison between experimental and theoretical values of the flow rate gain γ. Relative error $(\gamma_{\text{expt}} - \gamma_{\text{theory}})/\gamma_{\text{expt}}$ plotted as a function of the Péclet number β for the full model [Eq. (24), open circles and solid line], the limit $\beta \ll 1$ [Eq. (28), dots and dashed line], and the limit $\beta \gg 1$ [Eq. (30), squares and dash-dotted line]. Lines show smoothed data curves as a guide to the eye (averaged over 20 neighboring data points).

The flow rate gain γ can be expressed as

$$\gamma + 1 = \left[\frac{3}{2}\left(\frac{\Gamma}{\beta}\right)^{1/2} + 1\right]^{2/3} \tag{30}$$

$$= \left[\frac{3}{2}\left(\frac{12 L_p R T c^* L^2 D}{a^3 (u^*)^2}\right)^{1/2} + 1\right]^{2/3}, \tag{31}$$

shown in Fig. 4(a) as dashed lines. Equation (30) provides a simple approximation to Eq. (24) for large values of β/Γ, where the flow rate gain scales as $\gamma \propto (\Gamma/\beta)^{1/2}$. For $\beta \geqslant 1$ and $\Gamma \geqslant 1$ the error in Eq. (30) is typically less than 10% when compared to Eq. (24).

The flow rate gains predicted by Eqs. (28) and (30) are compared to the experimentally obtained values in Figs. 4(c) and 4(d), and the relative error $(\gamma_{\text{expt}} - \gamma_{\text{theory}})/\gamma_{\text{expt}}$ is plotted as a function of β in Fig. 5. While both Eqs. (28) and (30) show reasonable agreement between theory and experiment, the deviation between theory and experiment clearly depends on the value of β. Figure 5 thus illustrates that the parameter β plays an important qualitative role in determining the scaling of the flow rate gain γ with the parameters of the problem.

IV. CONCLUSION AND DISCUSSION

In this paper, we have studied the effect of concentration boundary layers on osmotic flows in cylindrical tubes with porous walls. By varying the inlet flow rate Q^*, inlet solute concentration c^*, and tube length L, we have experimentally documented the dependence of the flow rate gain γ [Eq. (1)] on these parameters.

To explain our experimental observations, we have developed a simple model. The model quantifies the change in axial flow velocity due to osmotic exchange of water across the tube wall, and gives a first approximation to the effect of concentration boundary layers [Eq. (24)]. We have compared theory and experiment with good results, as shown in Fig. 4(b).

Our theoretical predictions give interesting indications of how to develop and optimize devices that utilize osmotic pumps, such as membrane modules for forward osmosis applications based on hollow fibers [18,19]. To obtain the greatest osmotic effect, it is clearly desirable to maximize Γ and minimize β; see Fig. 4(a). This can be done in a number of ways, e.g., by using a long membrane tube ($\Gamma \propto L$, $\beta \propto L^{-1}$), or by injecting fluid slowly [$\beta \propto u^*$, $\Gamma \propto (u^*)^{-1}$]. The greatest potential for improvement, however, is in making the tube radius a as small as possible, since $\beta \propto a^2$ and $\Gamma \propto a^{-1}$. This increase in γ, however, will continue only as long as the back pressure due to viscous resistance, $\Delta p \simeq 8\eta L u^*/a^2$, remains small compared to the osmotic pressure $RTc^* \simeq 10^5$ Pa; cf. Eq. (2). For water ($\eta = 1$ mPa s) flowing at $u^* = 1$ mm/s in an $L = 1$ m tube, the two pressures are of equal magnitude when $a \simeq 100$ μm. This indicates that using sub-100-μm tubes in filtration devices is undesirable, although a more thorough analysis is needed to determine the optimum tube dimensions in the presence of viscous effects, and more generally nonlinear concentration effects such as deviations from the van't Hoff relation.

ACKNOWLEDGMENTS

The authors wish to thank Dr. Wang Rong, Singapore Membrane Technology Center, Nanyang Technological University, Singapore for kindly supplying the hollow fiber membrane and for helpful discussions. This work was supported by the Air Force Office of Scientific Research (Award No. FA9550-09-1-0188), the Materials Research Science and Engineering Center at Harvard University (MRSEC, NSF Grant No. DMR-0820484), and the Danish Council for Independent Research | Natural Sciences.

APPENDIX: MEMBRANE PERMEABILITY

The membrane permeability L_p was determined by applying a known hydrostatic pressure differential Δp across a membrane section of area A. By measuring the resulting flow rate Q, the permeability $L_p = Q/(A\Delta p)$ of the hollow fiber membrane was determined to be $L_p = (3.28 \pm 0.02) \times 10^{-12}$ m/s/Pa, consistent with values obtained from measurements on this type of membrane material [20].

[1] M. LaBarbera, Science **249**, 992 (1990).
[2] *Vascular Transport in Plants*, edited by N. M. Holbrook and M. Zwieniecki (Academic Press, New York, 2005).
[3] C. H. Nielsen, Anal. bioanal. chem. **395**, 697 (2009).
[4] J. Dainty, Protoplasma **57**, 220 (1963).
[5] T. J. Pedley and J. Fischbarg, J. Theor. Biol. **78**, 427 (1978).
[6] T. J. Pedley, J. Fluid Mech. **101**, 843 (1980).

[7] T. J. Pedley, J. Fluid Mech. **107**, 281 (1981).
[8] T. J. Pedley, Q. Rev. Biophys. **16**, 115 (1983).
[9] K. H. Jensen, T. Bohr, and H. Bruus, J. Fluid Mech. **662**, 197 (2010).
[10] G. K. Aldis, Bull. Math. Biol. **50**, 531 (1988).
[11] G. K. Aldis, Bull. Math. Biol. **50**, 547 (1988).
[12] P. Pohl, S. M. Saparov, and Y. N. Antonenko, Biophys. J. **75**, 1403 (1998).
[13] *CRC Handbook of Chemistry and Physics*, 93rd ed., edited by W. M. Haynes (CRC Press, Boca Raton, FL, 2012).
[14] R. Wang, L. Shi, C. Y. Tang, S. Chou, C. Qiu, and A. G. Fane, J. Membr. Sci. **355**, 158 (2010).
[15] S. Chou, L. Shi, R. Wang, C. Y. Tang, C. Qiu, and A. G. Fane, Desalination **261**, 365 (2010).
[16] T. Y. Cath, A. E. Childress, and M. Elimelech, J. Membr. Sci. **281**, 70 (2006).
[17] M. V. Thompson and N. M. Holbrook, Plant, Cell Environ. **26**, 1561 (2003).
[18] C. Tang, Y. Zhao, R. Wang, C. Hélix-Nielsen, and A. Fane, Desalination **308**, 34 (2013).
[19] Y. Zhao, C. Qiu, X. Li, A. Vararattanavech, W. Shen, J. Torres, C. Hélix-Nielsen, R. Wang, X. Hu, A. G. Fane, and C. Y. Tang, J. Membr. Sci. **423–424**, 422 (2012).
[20] L. Shi, S. Chou, R. Wang, W. Fang, C. Tang, and A. G. Fane, J. Membr. Sci. **382**, 116 (2011).